Geothermal Energy

RESEARCH

Open Access

Operational strategies to alleviate thermal impacts of the large-scale borehole heat exchanger array in Beijing Daxing Airport

Yaqian Ren[1,2,3], Yanlong Kong[1,2,3*], Yonghui Huang[1,2,3*], Shu Bie[4], Zhonghe Pang[1,2,3], Jichao He[4], Wei Yi[5], Bin He[5] and Jiyang Wang[1,2,3]

*Correspondence:
ylkong@mail.iggcas.ac.cn;
yh.huang@cup.edu.cn

[1] Key Laboratory of Shale Gas and Geoengineering, Institute of Geology and Geophysics, Chinese Academy of Sciences, Beijing, China
[2] Innovation Academy for Earth Science, Chinese Academy of Sciences, Beijing, China
[3] College of Earth and Planetary Sciences, University of Chinese Academy of Sciences, Beijing, China
[4] China IPPR International Engineering Co., Ltd, Beijing, China
[5] Capital Airports Holdings Co.,Ltd, Beijing, China

Abstract

Large-scale ground source heat pump (GSHP) systems are increasingly used for space heating and cooling. In comparison with smaller ones, large GSHP systems are often coupled with much more borehole heat exchangers (BHEs). Because of the intense thermal interactions between BHEs, they are more susceptible to significant ground temperature changes. Meanwhile, they possess the advantage that their operational strategies can be applied with a high degree of freedom, which presents chances to alleviate intense thermal interactions. In this study, we used a new performance indicator to access the effectiveness of GSHP operational strategies on alleviating thermal anomalies. The Daxing Airport GSHP system, contains 10,497 BHEs and is the largest in the world; therefore, it was selected as the test case for performance enhancement through operational strategies. We established a 2D model to predict ground temperature changes during the 50-year operation of the BHEs. First, it was revealed that the most severe thermal anomalies in the study area mainly occurred both within and between the BHE arrays, which should be mitigated. To alleviate the thermal anomalies caused by the thermal interactions of BHEs, operational strategies were applied by adjusting the cooling/heating starting sequence, setting time-dependent thermal loads, and reallocating thermal loads according to the position of the BHEs. Our study demonstrates that only the operation strategy that adjusts the cooling/heating starting sequence is beneficial for different BHE layouts, while the operational strategy that reallocates the thermal loads depending on BHEs position may be only effective for specific BHE layouts. In addition, our new performance indicator can be used to evaluate the effectiveness of the operational strategies and determine the spacing of adjacent BHE arrays. Therefore, it benefits the operation management of BHE array and design of BHE layout, and further guarantees the sustainable operation of the GSHP system.

Keywords: Large borehole heat exchanger system, Ground source heat pump, Performance indicator, Thermal anomaly, Operational strategy, Thermal interaction

Introduction

Ground source heat pump (GSHP) systems cool and heat buildings by circulating fluid through pipes in borehole heat exchangers (BHEs) to exchange energy with the ground. Owing to their environmental friendliness and sustainability, GSHP systems are witnessing an increasing market share in the global building sector (Bayer et al. 2019; Menegazzo et al. 2022; Noye et al. 2022; van der Zwaan and Dalla Longa 2019). According to statistics from the World Geothermal Congress 2021, the global installed capacity of GSHPs has increased nearly 40 times from 1995 to 2020, providing a total of 599,981 TJ of heating and cooling across 58 countries in 2019 (Lund and Toth 2021). In China, owing to market demand and policy encouragement, the application of GSHP systems has increased rapidly (Tang et al. 2021). To date, China has ranked first in the world in installed GSHP system capacity at approximately 20,000 MWth (Song et al. 2021).

A unique feature of Chinese market is that there are increasing number of large-scale GSHP systems, which are typically equipped with thousands of borehole heat exchangers (BHEs). Owing to the high demand for land surface area, the spacing of BHEs is typically narrow. According to the technical guidelines published by the Ministry of Housing and Urban–Rural Development of China (MOHURD) GB50366 (MOHURD 2009), a distance of 3–6 m must be maintained between BHEs. In practice, 4–5 m is the most common design for accommodating a large number of BHEs to provide a sufficient thermal load within a constrained space (Cai et al. 2019; Lucia et al. 2017). The compact arrangement of BHEs enhances thermal interactions and elevates ground temperature changes over the long-term operation of the GSHP system, which may hamper system efficiency and, in some cases, render the system unsustainable (Alaie et al. 2021; Schelenz et al. 2017). Fortunately, the large-scale GSHP system can strategically operate with many degrees of freedom, such as adjusting the operation time, circulation flow rate and inlet temperature. In this way, accumulated ground temperature changes could be mitigated and the performance of the BHE arrays can be improved.

Many studies have attempted to achieve high thermal efficiency by eliminating or mitigating the ground temperature changes through operational strategies (Arghand et al. 2021; Bayer et al. 2014; Beck et al. 2012). Ground temperature changes are caused by unbalanced seasonal heating and cooling demands and insufficient heat recharge from the surrounding subsurface (Choi et al. 2018; Luo et al. 2015; Yang et al. 2013; You et al. 2016). Therefore, one effective method is to balance the seasonal heating/cooling demand to avoid energy excess or deficit in ground. Meanwhile, reducing the amount of energy extraction and injection could be helpful. As the enormous heat extraction and injection can enlarge the thermal reach of individual BHEs, and leading to strong thermal interactions between BHEs; and the huge energy excess/deficit could be hardly compensated by the lateral heat flow (Koohi-Fayegh and Rosen 2012; Signorelli et al. 2004). The thermal interaction between adjacent BHEs is an important reason for the occurrence of thermal anomalies, particularly in the center of a BHE array (Kindaichi and Nishina 2018; Lazzari et al. 2010; Zhang et al. 2021), which can be addressed by enlarging the spacing between the BHEs. However, in real-world practice, this is not a viable option due to the land size constraints. Meanwhile, the number of BHE should be maintained in a certain range to meet the requirement of heating/cooling demand.

Operational strategies present a more practical approach for reducing thermal interaction to ensure the effective operation of large-scale GSHP systems.

In general, heating and cooling demand of buildings is supplied by multiple energy systems, for example, air-cooled chillers for cooling and boilers for heating. In this case, the run-time and thermal loads of BHEs can be adjust to ensure their sustainable operation. Many studies (Kerme and Fung 2020; Ma et al. 2020; Wang et al. 2022; Zhao et al. 2017) have investigated accessible strategies for reducing thermal interactions. For instance, operating a BHE intermittently provides more time for ground thermal recharge and reduces the mean ground temperature change (Arghand et al. 2021; Liu et al. 2016; Ma et al. 2021; Yang et al. 2014). Adjusting the thermal loads of BHEs to reduce the energy excess/deficit is a feasible approach, and the thermal load adjustment of BHEs in the central area is more common, since the most severe thermal anomalies mainly occurred in the center of a rectangular BHE array (Arghand et al. 2021; Yu et al. 2016).

Most previous studies have focused on the evaluation of operational strategies, but they are all related to small-scale GSHP systems up to hundreds of BHEs. A large-scale GSHP system with over 10,000 installed BHEs has not yet been investigated. In a large-scale GSHP system with thousands of BHEs, the placement of the BHEs is generally irregular, with different spacings between them, causing the complex thermal interactions between thousands of BHEs. In such cases, for large-scale BHE systems, the most severe thermal anomalies may not locate in the center of BHE arrays (due to irregular arrangement of BHEs) as it does in small-scale BHE arrays (Beck et al. 2013). Furthermore, the effective operational strategies proved by previous studies may have different, or even opposite, effects on the large-scale BHE system. Therefore, it is necessary to explore effective operational strategies for the operation of large-scale GSHP systems.

Motivated by the above considerations, a large-scale GSHP system at Daxing Airport was selected as the study case. A total of 10,497 BHE has been installed there, with an average thermal capacity of approximately 54 MWth, making it the largest GSHP system in the world. We established a 2D numerical model using the OpenGeosys (OGS) (Kolditz et al. 2012) simulator to predict the evolution of the ground temperature under the strategic operation and non-strategic operation. Furthermore, we employed a new indicator which could reflect the degree of thermal interactions outside of BHE arrays to assess the effectiveness of operational strategies. In this study, we aim to provide feasible operation strategies for the large-scale GSHP system, and give insight into the relationship between the effect of operation strategies and the distribution of thermal anomalies. The workflow described herein and operation strategies analysis will assist in the operation management of a large-scale GSHP system for long-term sustainable operation.

Methodology

Our workflow comprised two parts: first, we established a numerical model simulating the BHE operation under the operational strategies, using Daxing Airport as the study area. Second, we evaluated the effectiveness of the operational strategies according to the performance indicators.

Numerical model

In GSHP systems, the circulating fluid is injected into the ground through the BHE to store energy in summer, increasing the ground temperature around the BHEs. In winter, the heat is extracted, thereby decreasing the ground temperature.

If the energy extraction and storage are not seasonally balanced, the ground temperature continuously increases or decreases during the operation of BHEs. To predict ground temperature changes, we used OGS software to simulate the BHE-array operations. The OGS software contains different modules for 2D (Meng et al. 2019) and 3D (Cai et al. 2021) BHE heat-transport models. The 2D BHE heat-transport model module was applied in our study to keep the calculation cost and accuracy at an acceptable level. In the 2D model, the individual BHEs are represented as single nodes, where energy is injected and extracted, and the surrounding ground is treated as surface. The heat transport processes in grout and BHE pipes are ignored, and the ground thermal conductivity given should be an equivalent parameter which considering the thermal resistance of grout and pipes. For a site dominated by the heat conduction, the governing equation of the heat transport process in the subsurface is expressed as the following equation:

$$\frac{\partial}{\partial t}\left[\theta\rho_f c_{p,f} + (1-\theta)\rho_g c_{p,g}\right] T_g - \nabla \cdot \left(\Lambda_g \cdot \nabla T_g\right) = H_g, \tag{1}$$

where T_g is the ground temperature (K), Λ_g is the hydrodynamic thermo-dispersion tensor of the ground [W/(m·K)], ρ is the density (kg/m^3), c_p is the specific heat capacity [J/(kg·K)], and H_g is the thermal source term. The subscripts f and g represent the fluid and ground, respectively.

Performance indicators

Indicator z for a single BHE array

To compare different operational strategies, the performance indicator z proposed by Paly et al. (2012) and Bayer et al. (2014) was used. Paly et al. (2012) proposed the indicator z as the target to optimize the BHE thermal load, which could represent the maximum ground temperature changes. An effective operational strategy should minimize the maximum temperature change, since it would impact the efficiency of the BHE. Thus, the indicator z can be used to access the effectiveness of operational strategies. The indicator z consists of two parts: the maximum overall temperature change over the operation time t (Eq. 2), and the maximum temperature change in each time step l (Eq. 3). The secondary part is introduced considering that the maximum overall ground temperature may not be influenced by the load assignment in a certain period of time:

$$\max\left(\left|\Delta \overrightarrow{T}_{i,j}\left(t, \overrightarrow{q}\right)\right|\right) \forall (i,j,t) \in S, \tag{2}$$

$$\sum_{l=1}^{m} \max\left(\left|\Delta \overrightarrow{T}_{i,j}\left(l, \overrightarrow{q}\right)\right|\right), \tag{3}$$

where the $\Delta \overrightarrow{T}_{i,j}(t, \overrightarrow{q})$ is the subsurface temperature change at position (i,j) over the operation time t, with the temporal load pattern $\overrightarrow{q}$, and S is a set of two-dimensional points in coordinates (i,j) and time t, where m refers to the number of time steps.

Indicator z (Eq. 4) is formulated by combining the two parts with a weighting factor w, which maintains a high priority in the first part. In this study, $w = 0.01$, following the work of Bayer et al. (2014).

$$z = \max\left(\Delta \overrightarrow{T}_{i,j}(t, \overrightarrow{q})\right) + w * \sum_{l=1}^{m} \max\left(\Delta \overrightarrow{T}_{i,j}(l, \overrightarrow{q})\right). \tag{4}$$

Indicators $\overline{\Delta T_{i,j}}$ and z' for multi-BHE arrays

As mentioned above, z is controlled by the maximum change in the overall ground temperature. For a rectangular BHE array, the maximum ground temperature changes were often observed at the center of BHE arrays due to the thermal interactions between multiple BHEs under the imbalanced seasonal use (Cai et al. 2021; Chen et al. 2022; Liu 2020). In this case, z mainly reflects the degree of the thermal anomalies near the center of the array. However, for a large-scale GSHP system with multiple arrays, the thermal anomalies in the periphery of the array are less severe than that in the center, it can still be affected by the operation of neighbor arrays and become much more severe. Therefore, we added a new indicator $\overline{\Delta T_{i,j}}$ to evaluate the degree of thermal anomalies outside the BHE array. The temperature change at point (i,j) outside a BHE array generally decreases when it moves away from the center of a BHE array; the further away from the center of the BHE array, the smaller the temperature changes. Thus, the mean temperature changes outside the BHE array instead of the maximum value, was chosen to represent the thermal anomalies outside the BHE array, as follows:

$$\overline{\Delta T_{i,j}} = \frac{\sum_{i,j}^{S_2} \Delta \overrightarrow{T}_{i,j}(t, \overrightarrow{q}) * \Delta s}{A_{S_2}} \forall (i,j) \in S_2. \tag{5}$$

where S_2 is the interacting zone outside the BHE array, which is thermally affected (hereafter referred to as TAZ) of a BHE array; A_{S_2} is the area of the set of S_2; and Δs is the size of the grid at position (i,j).

z' is the defined as the combination of these three parts (Eq. 6). It should be noted that the parameter $\overline{\Delta T_{i,j}}$ could only be used when the thermal anomalies outside the BHE arrays could be determined. In our study, we chose a single BHE array in our study to simulate its operation and to calculate this indicator. This indicator was not applied for evaluating the thermal anomalies of Daxing Airport, but it was observed that the thermal anomalies outside the BHE are not affected by certain operational strategies based on the tests on the selected single BHE array. Although it is not the most severe thermal anomaly, it affects the efficiency of the GSHP system and should be considered.

$$z' = \max\left(\Delta \overrightarrow{T}_{i,j}(t, \overrightarrow{q})\right) + w * \sum_{l=1}^{m} \max\left(\Delta \overrightarrow{T}_{i,j}(l, \overrightarrow{q})\right) + \frac{\sum_{i,j}^{S_2} \Delta \overrightarrow{T}_{i,j}(t, \overrightarrow{q}) * \Delta s}{A_{S_2}}. \tag{6}$$

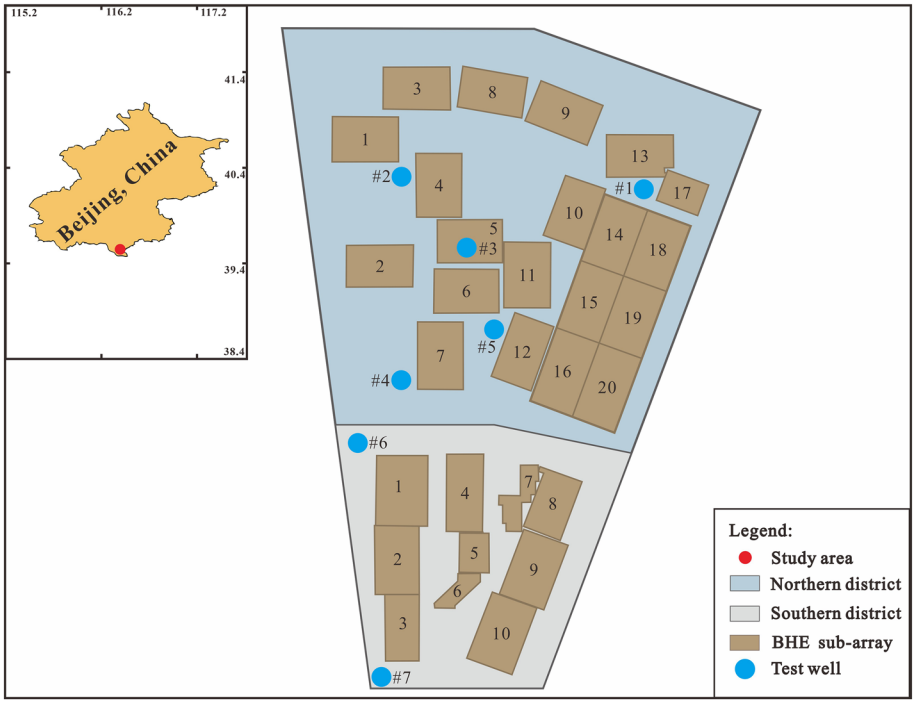

Fig. 1 Layout of the study area and arrangement of BHE arrays. The BHE system is divided into the northern and southern districts, with a total of 30 BHE arrays

Table 1 Detailed information of the BHE system

Items	Units	Northern district	Southern district
Number of BHE arrays		20	10
BHE type		Single U-type	Single U-type
Number of BHEs		7376	3121
Length of each BHE	m	140	120
Building seasonally thermal demand (heating application)	MW·h	69,393	34,550
Building seasonally thermal demand (cooling application)	MW·h	43,344	21,294
Ground density	kg/m^3	1514	1522
Ground heat capacity	J/kg·K	1480	1440
Ground thermal conductivity	W/(m·K)	1.62	1.62
Ground thermal diffusivity	m^2/s	1.0×10^{-5}	1.0×10^{-5}
Initial mean ground temperature	K	288.75	288.75

Model configuration

Project description

Our study area has an approximate size of 900 m × 1200 m, is located in the south of Beijing, China. It consists of 10,497 BHEs in a closed-loop system with a single U-type design. BHEs are connected in parallel to form 30 BHE sub-arrays, and the distances between adjacent BHEs are not uniform, varying from 4 to 5 m. The location of the study area and the specific layout of the BHE sub-arrays are shown in Fig. 1.

The BHE system can be divided into the northern and southern districts, which differ with regard to factors, such as BHE spacing and length (see Table 1). The arrangement

of the BHE arrays is more compact in the southern district than in the northern district. The BHE length in the north is much longer than that in the south. The main difference between the two districts is that they are used to heat and cool different buildings. The total seasonal thermal demand of the two districts differs owing to the different utilization times, thermal insulation, and covered area of these buildings. The detailed parameters of the BHE arrays are listed in Table 1.

Geological survey

Site investigations and thermal response tests (TRTs) were conducted by the building construction company. Because the final report of site investigations is not accessible in public, we briefly introduce the relevant information that serves as a foundation for numerical modeling.

Regional geological surveys revealed that the study area was covered by approximately 300 m of Quaternary sands, and the depth of the groundwater table was approximately 27 m. The subsurface was mainly composed of clay, silt, medium sand, coarse sand, and gravel, and the thickness of each formation differs slightly between the two districts. Figure 2 summarizes the stratigraphic layering within the BHE length, which was 140 m in the northern district and 120 m in the southern district. Based on the thickness and the physical parameters of each formation (Table 2), the equivalent ground physical parameters were calculated, and are listed in Table 1.

A previous study (Sun 2021) reported that the groundwater flow direction is predominately southeastward, and the flow velocity was between 0.008 and 0.04 m/d. In this

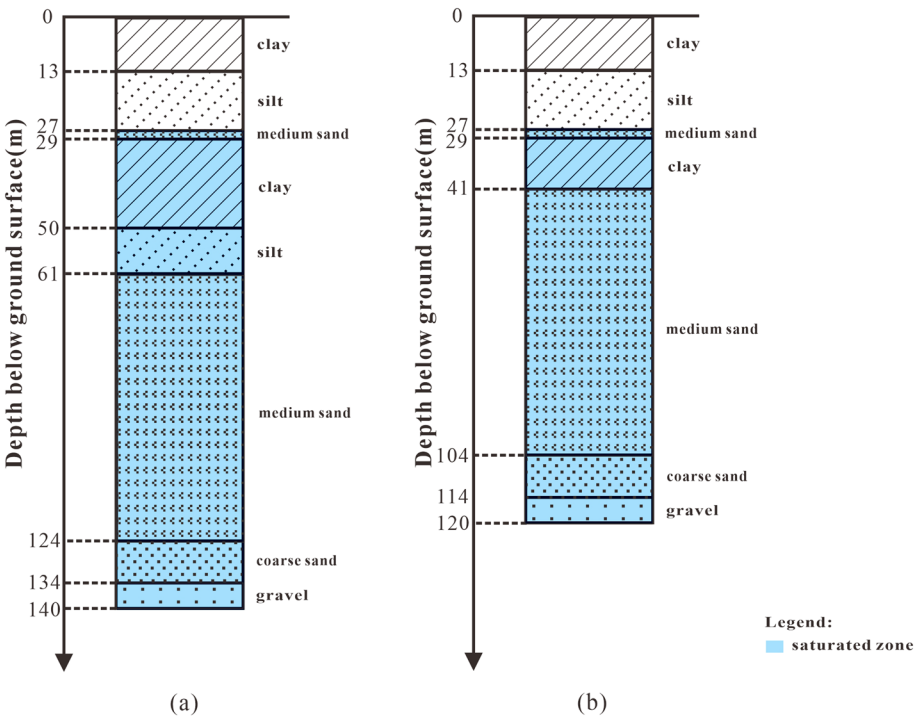

Fig. 2 Stratigraphy of the (**a**) northern and (**b**) southern district in Daxing airport

Table 2 Physical parameters of formations

Rock type	Specific heat capacity (kJ/kg·K)		Porosity		Density (kg/m^3)		The water content	
	Vad.	Sat.	Vad.	Sat.	Vad.	Sat.	Vad.	Sat.
Clay	1.30	1.38	0.47	0.47	1.9×10^3	1.95×10^3	0.23	0.28
Slit	1.40	1.40	0.40	0.40	1.88×10^3	1.92×10^3	0.18	0.20
Medium sand	1.05	1.05	0.35	0.35	1.95×10^3	1.95×10^3	0.16	0.18
Grit/Coarse sand	1.05	1.05	0.38	0.38	1.95×10^3	1.95×10^3	0.14	0.20

Vad. represents Vadose zone, Sat. represents saturated zone

case, the impact of the groundwater flow was negligible, and the heat transport process was assumed to be dominated by heat conduction.

Based on the data of in-situ TRTs provided by the building construction company, the thermal conductivity and initial mean ground temperature of the ground were estimated. A TRT is a process that forces the closed circulation of a heat carrier that is heated constantly (Sapińska-Sliwa et al. 2019). Six TRTs were performed in six different test wells (#2–#7), and the results were evaluated based on the Kelvin's line source theory. Through solving and applying the proposed transformation and substitution (Sapińska-Sliwa et al. 2019), it can be written as

$$T(r,t) - T_0 = \frac{q_{sp}}{4 \cdot \pi \cdot \lambda_{eff}} \left[\ln\left(\frac{4 \cdot \alpha_{eff}}{r^2} \right) + \ln(t) - \gamma \right] \tag{7}$$

where $T(r,t)$ is the temperature at distance r at time t, T_0 is the undisturbed ground temperature, q_{sp} is heating power per unit depth,λ_{eff} is the effective thermal conductivity, α_{eff} is the effective thermal diffusivity, and γ is the Euler–Mascheroni constant (0.57722).

From Eq. (7), the gradient of the regression line of the TRT measurement ϕ was equal to $\frac{q_{sp}}{4 \cdot \pi \cdot \lambda_{eff}}$ when the mean temperature of the fluid was plotted against the logarithm of time [ln(t)]. By determining the heating power and gradient, the λ_{eff} can be calculated as follows:

$$\lambda_{eff} = \frac{q_{sp}}{4 \cdot \pi \cdot \phi} \tag{8}$$

The value of q_{sp} equals to the heating power P divided by the BHE length, which is 140 m in our test. The heating power P can be calculated from the dependence $P = Q \cdot \rho_f \cdot c_{p,f} \Delta T$, where ΔT is the fluid temperature difference between the inlet and outlet, Q is the flow flux, ρ_f is the fluid density, and $c_{p,f}$ is the specific heat capacity of fluid. We selected TRTs that met the demand that of a duration time > 30 h (Sapińska-Sliwa et al. 2019) and had a relatively high correlation ($r^2 > 0.96$) (as shown in Fig. 3). Detailed parameters are listed in Table 3. Finally, the thermal conductivity was determined to 1.62 W/(m·K), which is the mean value of the results of the four TRTs.

Before construction, the undisturbed ground temperature at the initial stage was determined using the TRT. In contrast to TRTs conducted to determine the effective thermal conductivity, the heater did not heat the fluid flowing out of the BHE. By continuously circulating the fluid in the pipes of the BHE, the circulated fluid temperature gradually approached the ground temperature, and finally, no heat exchange occurred

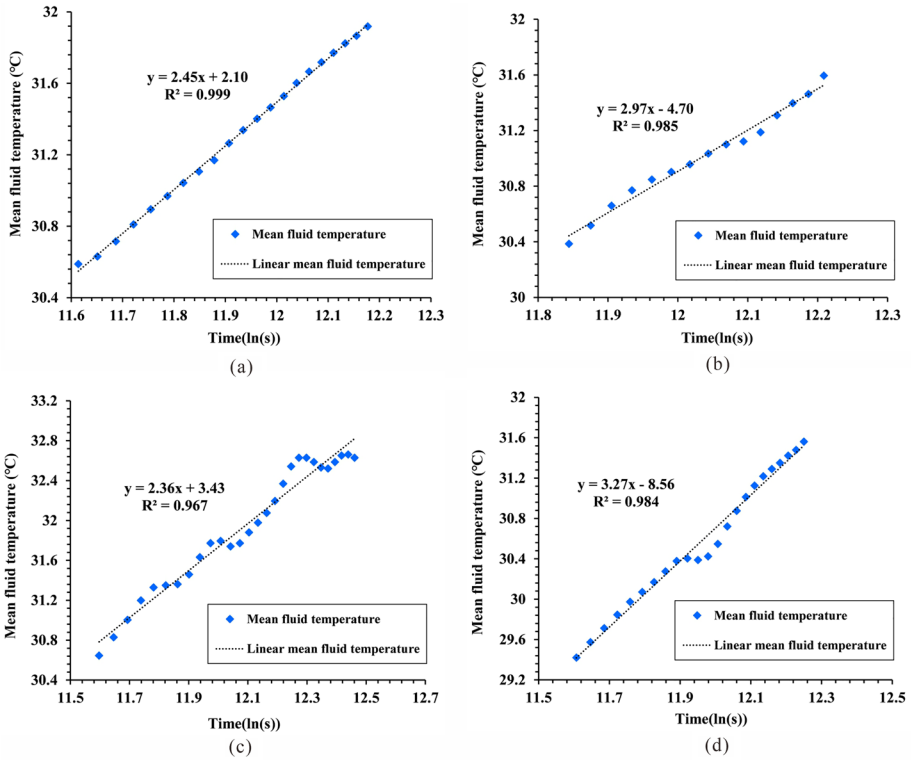

Fig. 3 Variation of mean temperature of fluid flowing out of BHEs with logarithm of time

Table 3 Detailed parameters measured from the TRTs

Well	Mean temperature difference (K)	Flow flux (m^3/h)	Heating power (W)	Heating power/BHE length (W/m)	Regression curve	Thermal conductivity coefficient [W/(m·K)]
#3	4.19	1.52	7430.3	53.1	y = 2.45x + 2.10	1.72
#4	4.36	1.55	7884.3	56.3	y = 2.97x − 4.70	1.51
#5	4.50	1.55	8137.5	58.1	y = 2.36x + 3.43	1.96
#6	4.28	1.50	7490.0	53.5	y = 3.27x − 8.56	1.30

between the ground and circulated fluid. Therefore, the fluid temperature was the same as the ground temperature when the fluid temperature was stabilized. In our test, the fluid temperature was maintained at 288.75 K for approximately 24 h.

Model setup

To predict ground temperature changes under different strategic operations, we established a 2D model to simulate the operation of the BHE array. Because of the extensive domain size, we established separate meshes for the southern and northern districts. As illustrated in Fig. 4, the size of the triangular elements varies from 1 to 5 m^2 in the two districts because of the compact arrangement of the BHEs, with a refined mesh in the vicinity of the BHEs, and a coarser mesh to the edge of the domain. Finally, 2,179,945 elements and 1,087,975 nodes were obtained. The adopted mesh sizes were verified to

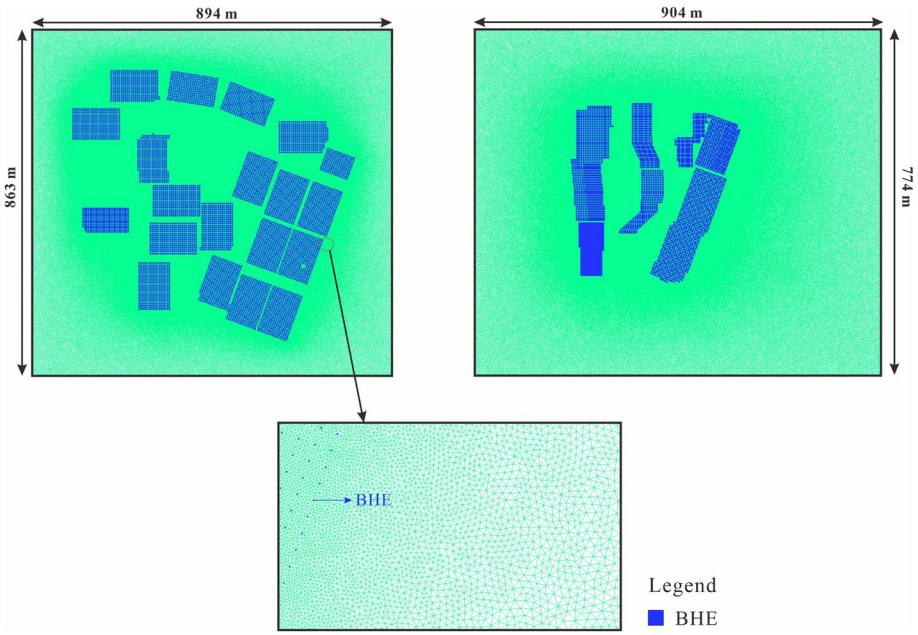

Fig. 4 Overview of the 2D finite-element mesh with its spatial discretization

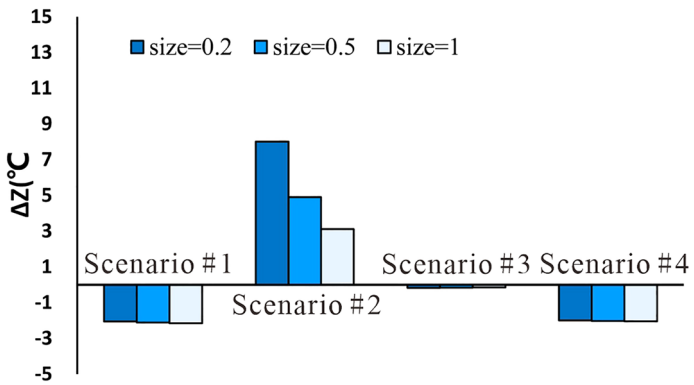

Fig. 5 Comparison of Δz with different mesh sizes. Δz is the performance indicator difference between the strategic operation (Scenarios #1–#4) and non-strategic operation (Scenario #0)

ensure the accuracy of the model. A single BHE sub-array (the sixth BHE sub-array in the northern district), consisting of 384 BHEs, was chosen as an example for the mesh-independence test. As illustrated in Fig. 5, with the decrease in mesh size from 1 to 0.2 m^2, the performance indicator remained unchanged in Scenarios #1, #3, and #4 (Scenarios 1–4 are described in Section 'Scenario descriptions'). However, it visibly decreased in Scenario #2, but remained positive. This is considered to have no effect on our results, because a positive value declares that this operational strategy is still harmful to BHE operation as the mesh size increases. Besides, a previous study has demonstrated that the error of numerical model will converge with more refined meshes (Meng et al. 2019). Thus, an accurate estimate of the effectiveness of the operational strategy was obtained when the mesh size is 1 m^2.

In the 2D model, appropriate simplifications and assumptions on site characterization were made, that are, the subsurface was assumed to be homogeneous and isotropic, while the focus is on the evaluation of strategic operations. The assumption is valid as study area is covered by approximately 300 m of Quaternary sands, which are uniform in the lateral direction; and groundwater temperature monitoring also showed that vertical temperature variations are less than 2 K.

Initial and boundary conditions

For the initial condition, the undisturbed ground temperature was set to 288.75 K based on the TRT. A Neumann boundary with no heat flux was set as the side boundaries, and large domain sizes was provided to ensure that the thermal plume caused by the BHE operation did not interfere with the boundary of the model. In addition, the heat fluxes across the top and bottom were negligible because of the low temperature gradient (0.014 K/m) and thermal conductivity [1.62 W/(m·K)]; thus, the surface of the model domain was set to be Neumann boundary with no heat flux. As for the boundary condition for the BHEs, the nodes representing the BHEs became active as thermal sinks/sources with constant or time-dependent thermal load during heating/cooling periods, and are treated as inactive during recovery phases.

The specific thermal loads of the BHE were determined from the totally heating/cooling demands (listed in Table 1). Under the premise that the COP was constant and all BHEs operate together with an equally distributed load, the specific thermal load for a single BHE in the northern district was 16.76 W/m in summer and − 17.59 W/m in winter. In the southern district, the corresponding values were 22.70 W/m in summer and − 24.15 W/m in winter.

Scenario descriptions

In Daxing airport, the building heating and cooling demand are supplied by multiple systems, including gas-burning boilers, waste heat from flue gas, and the GSHP system. Thus, the operation of large-scale GSHP can be strategically adjusted with a high degree of freedom. This allows a single BHE array or parts of it to operate alone, rather than all BHEs operating simultaneously. In addition, a part of the BHE array is controlled by a single pump; therefore, its heating extraction/injection rate (which is related to the thermal load) can be changed by adjusting the flow rate of the circulated fluid. However, an operational strategy that should be applied to achieve high efficiency and reduce thermal anomalies remains an issue. This study aims to evaluate the effects of different operational strategies and improve the performance of large-scale GSHP. We simulated five scenarios as listed in the following.

1. The baseline case (non-strategic operation) was marked as Scenario #0. In this case, the GSHP system began operation on September 16 by heating followed by cooling. The specific thermal load was maintained at constant values (Table 4).
2. In Scenario #1, the GSHP system began operation with cooling first, and shifted the starting date from September 16 to March 15.
3. The operational strategy "adjustment of BHE load" determines whether the BHE load is constant or variant. While the constant loads were modelled in Scenario #0, a vari-

Table 4 Operation time and COP of BHE

Season	Date	COP	Specific thermal load of the Northern district (W/m)	Specific thermal load of the Southern district (W/m)
Heating period	Nov. 12–Mar. 14 (123 days)	5.31	− 17.59	− 24.15
Cooling period	May 15–Sep. 15 (124 days)	4.40	16.76	22.70

able load was imposed in Scenario #2. Figure 6 shows the evolution of the specific thermal load applied in Scenario #2.

4. The operational strategy "reallocating the BHE loads according to the position of BHEs" determines whether the thermal load of BHEs in different regions should be the same or different. This strategy involved strategically reallocating the total thermal demand to different BHEs depending on their position. Specifically, the area where the severe thermal anomalies exist will bear less thermal load. In Scenario #3, all BHE arrays were divided into two-regions: subregions 1 and 2, as shown in Fig. 7. In this way, the central BHEs and peripheral BHEs were divided into the same region, subregion 2. We divided in this way based on the result of Scenario #0, which showed that the severest thermal anomalies occurred on the subregion 2. Both subregions operated together with different distributed BHE loads. Specifically, subregion 2 was set to have a higher cooling load compared to subregion 1 (the specific thermal load of BHE is listed in Table 5), to balance the amount of heat release and heat extraction

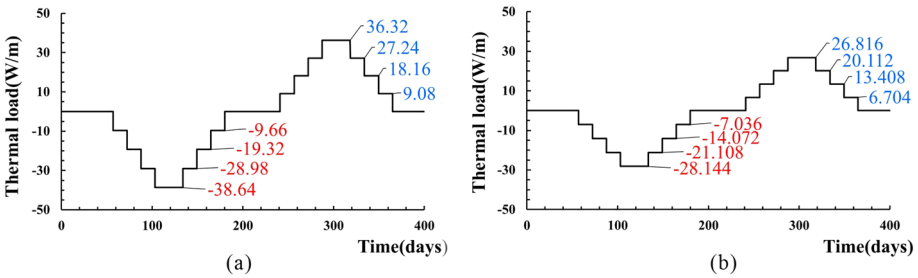

Fig. 6 Variation of the specific thermal loads in the northern district (**a**) and southern district (**b**). The negative value represents the heating load in winter (Nov.12–Mar.14), while the positive value refers to the cooling load in summer (May15–Sep.15)

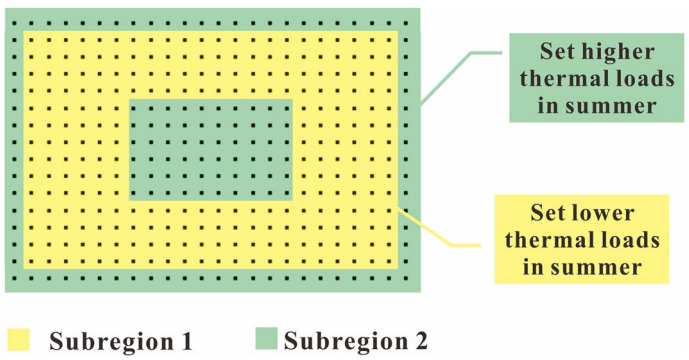

Fig. 7 Schematic illustration of the operational strategy that thermal load reallocation

Table 5 Specific thermal load of BHEs in Scenario #3 when $\eta = 0.96$

Region	Season	Specific thermal load of the Northern district (W/m)	Specific thermal load of the Southern district (W/m)
Subregion 1	Heating period	− 17.59	− 24.15
	Cooling period	16.42	22.24
Subregion 2	Heating period	− 17.59	− 24.15
	Cooling period	17.10	23.16

Table 6 Operational parameters of simulated Scenario #0–#4

Scenario ID	Start time	BHE load	Load ratio, η
#0	Sep.16	Constant	1
#1	Mar.15	Constant	1
#2	Sep.16	Variable	1
#3	Sep.16	Constant	0.96
#4	Mar.15	Constant	0.96

of subregion 2. The load ratio η represents the ratio of the thermal load in subregion 1 over the load in subregion 2, which is written as

$$\eta = \frac{(qh/qc)_{\text{subregion1}}}{(qh/qc)_{\text{subregion2}}}. \tag{9}$$

where q_h and q_c are the specific thermal loads of a single BHE in heating and cooling period.

5. According to the effect of the above operational strategies (Scenarios #1–#3), Scenario #4 describes the strategic operation integrating the effective operational strategies based on the results of Scenarios #0–#3; that is, if the model results show that GSHP start in winter can alleviate thermal anomalies, this operation mode will be adopted in Scenario #4. The operational parameters of all scenarios are summarized in Table 6.

   For comparison, all above strategies had the same amount of annual heat injection and heat extraction (Table 1).

Results and discussion

Results of operational strategies

In this section, we analyzed the effectiveness of the operational strategies based on the amount of ground temperature changes and resulting performance indicators. The minimum ground temperature reflects the degree of the most severe cold accumulation; therefore, in this study, the evolution of the minimum temperature was presented to show the change in thermal anomalies after strategic operation. Figure 8 shows that the minimum temperature fluctuated in all scenarios because of alternating heating and cooling. In addition, the minimum temperature of in all scenarios shows a visibly decreasing trend, as the energy deficit in the subsurface cannot be completely

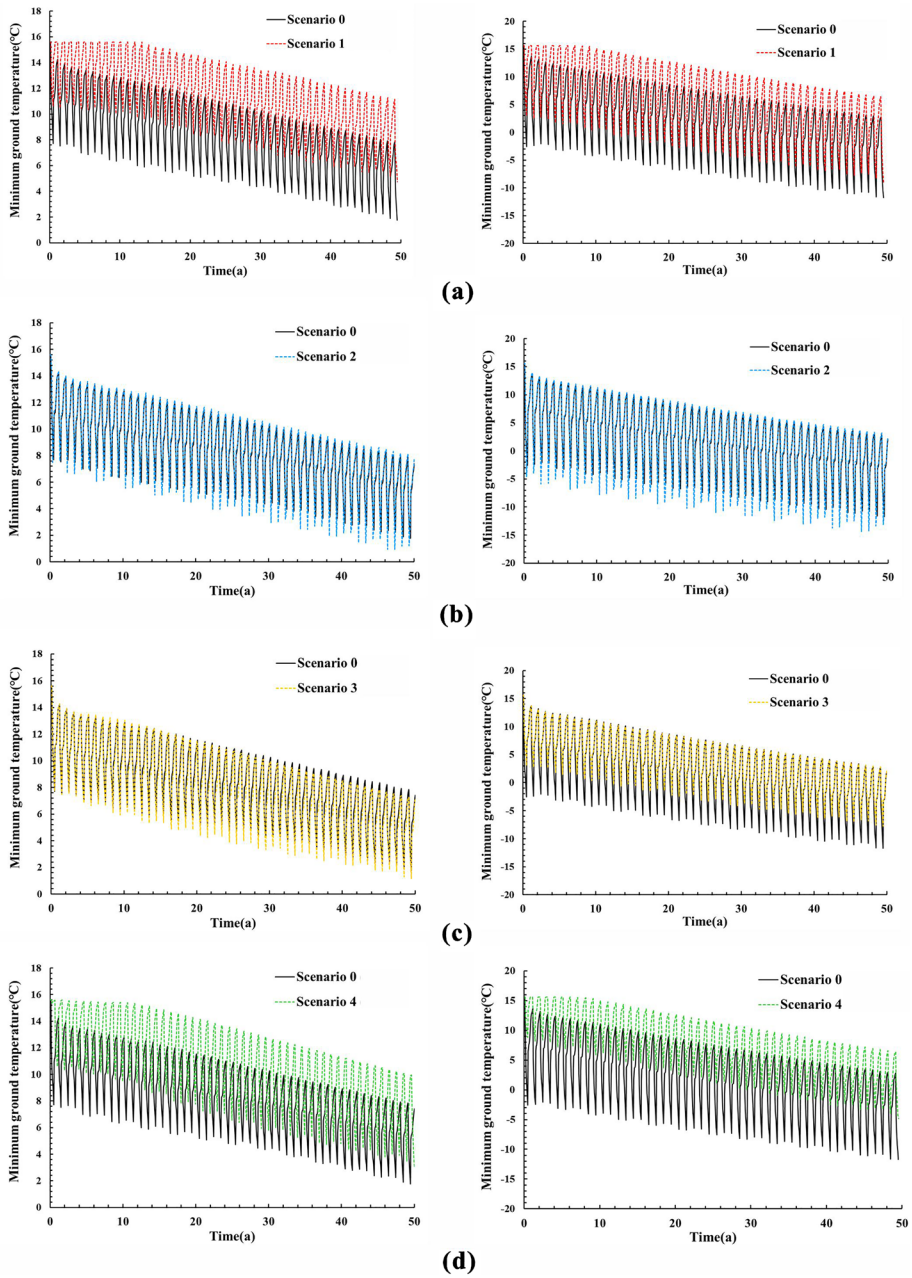

Fig. 8 Evolution of the minimum ground temperature simulated in Scenarios #0–#4. The left graphs show the results for the northern district, while the right ones are for the southern district. The downward trend of ground temperature indicates the occurrence of cold accumulation

compensated for by natural thermal flux recharge. This phenomenon indicates that the trend of severe cold accumulation cannot be prevented through operational strategies.

However, operational strategies can relieve severe cold accumulation to a certain extent. As illustrated in Fig. 8a, the minimum ground temperatures were approximately 4.1 K (the average of the maximum ground temperature differences in the 50-year operation period) higher in Scenario #1 than in Scenario #0, which indicated that strategic adjustment of the starting sequence can successfully alleviate cold accumulation. This

results of Scenario #1 is consistent with previous works (Arghand et al. 2021; Liu 2020): the "adjustment of starting sequence" could improve the ground temperature and compensate for the energy deficit in the subsurface.

Figure 8b shows that the thermal interactions of the BHEs were strengthened by adjusting the BHE load (Scenario #2), which was inconsistent with the result of previous study based on the lattice arrangement of BHEs (Paly et al. 2012). The failure of variable BHE load to improve the performance of the GSHP system may be due to the linear variation of the BHE load. The high thermal load variation gradient that we set may be the main reason for this. The highest load has a significant impact on the heat transport balance of the ground, and this impact cannot be recovered from the subsequent decreased thermal load.

The changes caused by the reallocation of the thermal load differed between the southern and northern districts. The strategy that reallocates the thermal load of BHEs in areas, where severe thermal interaction has a positive effect on alleviating thermal anomalies in the southern district; in contrast, it has an opposite effect for the northern district. The effectiveness of these operational strategies depends on the location of thermal anomalies. As depicted in Fig. 9, the maximum temperature changes, marked by pink dots, occurred near the center and outside the BHE arrays in the southern district. However, this only occurred outside the BHE array in the northern district. The maximum ground temperature changes occurring in the middle of a BHE array are expected, which has been revealed in many studies (Bayer et al. 2014; Lazzari et al. 2010). The severe thermal interactions of BHEs cause a significant ground temperature decline. Following the same reason, the significant ground temperature changes outside the BHE arrays are a result of the thermal interactions between the BHE arrays. The compact arrangement of the BHE arrays results in this outcome. The main question is, why the operational strategy has different effects on the two districts and what affects the effectiveness of the operational strategy; furthermore, previous studies that improved the efficiency of the BHE system through strategic operation based on the regular BHE arrangement, which may not be feasible for large BHE systems with specific layouts.

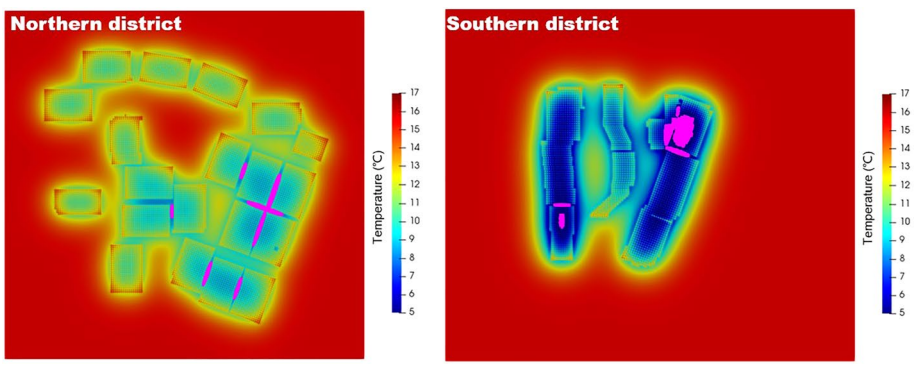

Fig. 9 Distribution of ground temperature after a 50-year-long period operation in Scenario #0. The 3000 mesh nodes with the lower temperature are marked by the pink dots. In the northern district (**a**), the most severe cold accumulation occurs outside BHE arrays, and occurs inside and outside of the BHE arrays in the southern district (**b**)

According to the above analysis, the strategy that starts with cooling first can be used in two districts to mitigate thermal anomalies. The operational strategy for thermal load reallocation is effective only for the southern district. Scenario #4 refers to the operational strategy that adjusts the starting sequence and reallocates the thermal load, which can mitigate thermal anomalies in the southern district. For comparison, the northern district adopted the same operating method.

Figure 8d shows that the cold accumulation in Scenario #4 was less severe than that in Scenario #0, with a significantly higher temperature by 5.6 K (the average of the maximum ground temperature differences in the 50-year operation period). It is expected that thermal anomalies can be significantly alleviated through the integration of effective operational strategies. Compared with the maximum ground temperature changes, the performance indicator Δz directly reflects the effect of combined operational strategies. A negative value of Δz indicates that the operational strategies are effective, and vice versa, and a better benefit will be achieved with a decline in Δz. From Fig. 10, it was obvious that thermal anomalies in the southern district were further alleviated by "reallocation of thermal load (Scenario #3)" and "integrated operational strategy (Scenario #4)"; and the integrated operational strategy had a better effect on it.

Discussion

Affected zone of "reallocation of thermal load" operational strategy

To investigate why the operation strategy that "reallocation of thermal load" operational strategy has different effects on the two districts. We conducted extended numerical experiments to determine the "affected zone" of this strategy**.** The single BHE array (the sixth BHE sub-array in the northern district) used to carry out mesh-independence tests was chosen as the case for the experiments. The non-strategic operation scenario and strategic operation scenario are constructed corresponding to the Scenarios #0 and #3. The non-strategic scenario had the same parameters as Scenario #0, and the operational strategy scenario reallocated the thermal load between the BHEs with a load ratio of 0.93.

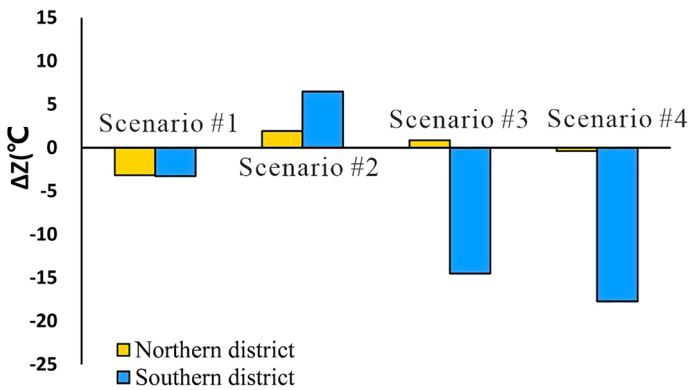

Fig. 10 Comparison of z difference (Δz) between Scenario #0 and Scenarios #1–#4. The negative value indicates the cold accumulation is minimized, and vice versa, The strategies simulated by Scenario #1, #3 and #4 could alleviate the cold accumulation with negative values

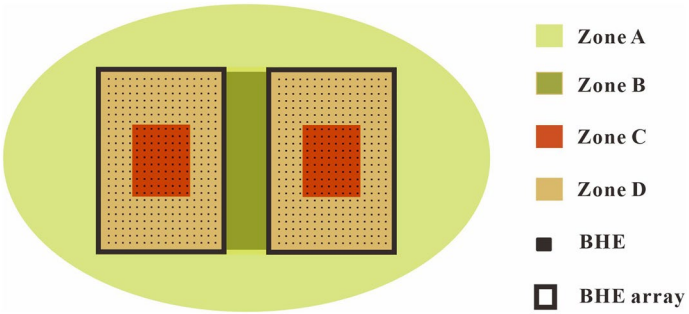

Fig. 11 Schematic diagram of definition of Zone A–D. Zone A to D refer to the zone outside BHE arrays, the zone between BHE arrays, the center of BHE arrays, and the zone inside BHE arrays, respectively

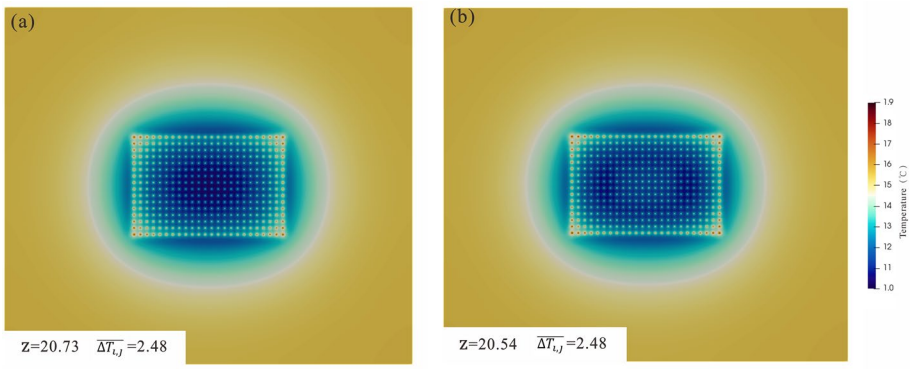

Fig. 12 Comparison of the temperature distribution between the non-strategic operation (**a**) and the strategic operation (**b**). The cold accumulation in Zone C is visibly alleviated with the lower z and temperature value through the optimization, while the cooling in Zone A has little change with the similar $\overline{\Delta T_{i,j}}$

For easier description in the following section, we categorize the model domain into several zones from A to D, as shown in Fig. 11. As depicted in Fig. 12, the thermal anomalies in Zone C were obviously relieved, while the thermal anomalies in Zone A remained unchanged. The performance indicator $\overline{\Delta T_{i,j}}$ also exhibited that thermal anomalies outside the BHE arrays (Zone A) have negligible changes. In contrast, the value of performance indicator z declined after the application of the operational strategy. As stated above, the value of z is negatively correlated with the degree of thermal anomalies, which includes the most severe cold accumulation in Zones C, and $\overline{\Delta T_{i,j}}$ reflects the degree of severest cold accumulation in Zone A. Therefore, we came to the conclusion that the affected zone of "reallocation of thermal load" strategy does not reach to the outside of BHE array.

Thermal anomaly outside BHE arrays

Several studies (Bayer et al. 2014; Chen et al. 2019; Gultekin et al. 2019; Zhang et al. 2021) have discovered that the most severe thermal anomalies generally occur in Zone C, which can be explained by the significant thermal interaction between the BHEs. In general, the most severe thermal anomalies are caused by the limited spacing of adjacent BHEs and the heating/cooling load, which causes the overlap of the TAZ of BHEs during

operation. Thus, for a BHE array, the spacing between the BHEs should to be larger to avoid the overlap of the TAZ (Daemi and Krol 2019). Many countries have guidelines for the spacing between BHEs, most of which range from 3 to 6 m (ASHRAE 2021; Miglani et al. 2018; MOHURD 2009; VDI 2019).

In this study area, thermal anomalies occurred in Zone A due to thermal interactions, but this differed between the BHE arrays. As illustrated in Fig. 10, the most severe thermal anomalies occurred in Zone A between the BHE arrays with a narrow spacing. The distance between the BHE arrays is also a key factor for avoiding thermal interactions to prevent the occurrence of thermal anomalies, especially for large-scale GSHP. Owing to the increase in large-scale GSHP, the design and arrangement of BHE arrays are important. In our work, the distance between adjacent BHE arrays in Daxing airport is larger than 13 m in the northern district and from 5.4 m to 19.6 m in the southern district. This spacing is short for the study area; however, the optimal length needs to be determined.

The TAZ of the BHE array was studied to determine the optimal distance between the BHE arrays. The 1.5 K TAZ (the zone where temperature change is over 1.5 K) can reach 27.2 m in the north–south (NS) direction and reach 32.6 m in the east–west (EW) direction, with the maximum temperature being ca. 5 m away from the BHE array (Fig. 13). If the BHE arrays are closely arranged, the interactions between the arrays strengthen the thermal anomaly. To avoid overlap of the TAZ of BHE arrays, the distance between BHE arrays is recommended to be at least 5 m and preferably 27.2 m in NS direction and 32.6 m in EW direction, although this will require a significant increase of initial financial investment.

The results obtained from this study are moderate by the hypothesis that the COP and thermal load of BHE (except for Scenario #2) were constant, as those parameters are affected by the change of ground temperature. Instead of precisely predicting the efficiency and thermal performance of the system, the focus of this work is to access the effectiveness of operational strategies under the given energy extraction and injection, which is based on the ground temperature changes in response to the operational strategies. Significant ground temperature changes should be avoided as this could mitigate the efficiency of the heat pump. This idea has been widely used in

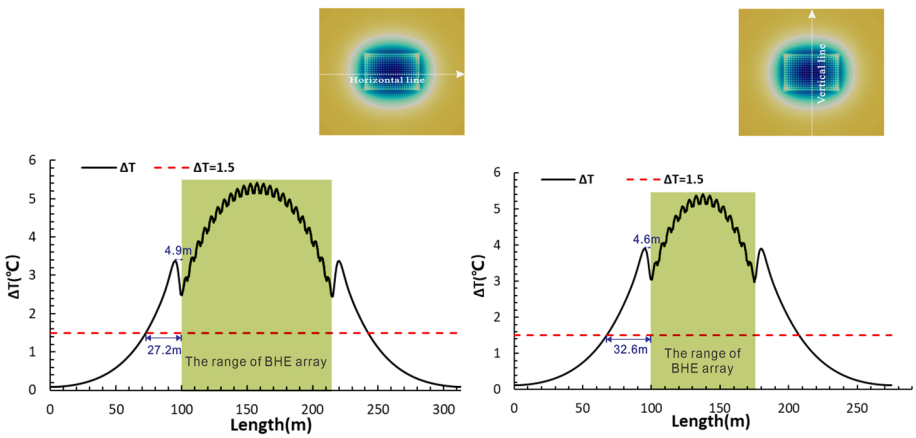

Fig. 13 Temperature changes distribution of section line after 50-year operation in Scenario #0. The TAZ of a BHE array reaches to 27.2 m far away from the BHE in NS direction, and reaches to 32.6 m in EW direction

optimizing the operational parameters, designing the arrangement of BHE, and analyzing the thermal impacts of BHE operation from environmental perspectives (Peter et al. 2014; Beck et al. 2013). Such gain from the hypothesis and specific BHE layout of case study is limited. Our main contribution here is to realize that the distance between BHE arrays is a critical parameter for the arrangement of BHE array; and demonstrate that the operational strategies could have contrary effect on the operation of GSHP systems according to the arrangement of BHEs.

Conclusions

In this study, the ground temperature changes under different operation strategies of a large-scale GSHP system were investigated by conducting numerical simulations, and the effectiveness of operational strategies was evaluated based on the simulation results. Four different operational strategies were provided to improve the performance of the GSHP system by alleviating thermal anomalies in the ground. To compare the results of the operational strategies, a new performance indicator was developed to reflect the effect of the operational strategies on thermal anomalies outside the BHE array. The major findings of this study are as follows.

(1) The thermal anomalies outside the BHE arrays are caused by strong thermal interactions between the BHE arrays, and the narrow spacing between the arrays is the main cause of these thermal interactions.
(2) For the BHE array examined in this study, the 1.5 K TAZ can extend to 27.2 m in NS direction and 32.6 m in the ES direction after a 50-year operation, and the highest thermal anomaly was 4.6 m away from the BHE array. This suggests that the distance of adjacent BHE arrays should be at least more than 4.6 m but ideally more than 27.2 m in the NS direction and 32.6 m in the ES direction.
(3) The tendency of the ground temperature to decrease is unavoidable in the operational strategy, but operational strategies can alleviate the most severe thermal anomalies. Adjustment of the starting sequence could help further alleviate thermal anomalies in the southern district, while the operational strategy of thermal load reallocation will be effective in certain cases. A typical example is the different effects of this strategy on the northern and southern districts, which may be accounted for the different BHE layouts.
(4) Thermal load reallocation could improve the performance of the GSHP system by alleviating the thermal anomalies in the BHE arrays, while not affecting the thermal anomalies outside the BHE arrays.

In the study area, a severe temperature change of ca. 27.3 K outside the BHE array was identified in the large GSHP system. This finding indicates the ideal distance between BHE arrays to avoid severe thermal anomalies. In addition, the new performance could help to access the effectiveness of operational strategies and determine the spacing of adjacent BHE arrays. Thus, our work will help in designing the placement of BHEs and the strategic operation of BHE systems to avoid thermal anomalies.

Abbreviations

BHEs	Borehole heat exchanger
COP	Coefficient of performance
EW	East–west
GSHP	Ground source heat pump
NS	North–south
OGS	OpenGeosys
TAZ	Thermally affected zone
MOHURD	Ministry of Housing and Urban–Rural Development of China

Symbols

$\overline{\Delta T_{i,j}}$	Performance indicator
Λ_g	Hydrodynamic thermo-dispersion tensor of the ground [W/(m·K)]
A_{S_2}	Area of the set of S_2
H_g	Thermal source term
S_2	Interacting zone outside the BHE array
T_0	Undisturbed ground temperature (K)
T_g	Ground temperature (K)
q_h	Specific thermal load of a single BHE in heating period (W/m)
q_c	Specific thermal load of a single BHE in cooling period (W/m)
q_{sp}	Heating power per unit depth (W/m)
z'	Performance indicator
α_{eff}	Effective thermal diffusivity (m^2/s)
λ_{eff}	Effective thermal conductivity [W/(m·K)]
ΔT	Fluid temperature difference between the inlet and outlet (K)
Δs	Mesh size (m^2)
$c_{p,f}$	Specific heat capacity of fluid [J/(kg·K)]
$c_{p,g}$	Specific heat capacity of ground [J/(kg·K)]
P	Heating power (J)
Q	Flow flux (m^3/s)
S	Set of two-dimensional points in coordinates (i, j)
γ	Euler–Mascheroni constant (0.57722)
$\Delta \overrightarrow{T}_{i,j}(t, \overrightarrow{q})$	Temperature changes at position (i, j) over the operation time t, with the temporal load pattern $\overrightarrow{q}$ (K)
ρ_f	Fluid density (kg/m^3)
ρ_g	Ground density (kg/m^3)
$T(r, t)$	Temperature at distance r at time t (K)
m	Number of time steps
w	Weighting factor
z	Performance indicator
η	Load ratio
ϕ	Gradient of the regression line of the TRT measurement

Acknowledgements
This project has received funding from Beijing New Airport Construction Headquarters and the Youth Innovation Promotion Association of CAS (2020067).

Author contributions
YR, YK and YH: conceived this study, created the models, and wrote the paper. SB, JH, WY, and BH: performed the experiments and provided monitoring data in the study case. ZP and WY: contributed to improving the paper. All authors read and approved the final manuscript.

Funding
This work was funded by the Beijing New Airport Construction Headquarters and the Youth Innovation Promotion Association of CAS (2020067).

Availability of data and materials
The data sets generated and analyzed during the current study are available from the corresponding authors on reasonable request.

Declarations

Consent for publication
Not applicable.

Competing interests
The authors declare that they have no competing interests.

Received: 16 March 2023 Accepted: 22 May 2023
Published online: 07 June 2023

References

Arghand T, Javed S, Trüschel A, Dalenbäck JO. Influence of system operation on the design and performance of a direct ground-coupled cooling system. Energy Build. 2021;1:234.

Alaie O, Maddahian R, Heidarinejad G. Investigation of thermal interaction between shallow boreholes in a GSHE using the FLS-STRCM model. Renew Energy. 2021;175:1137–50.

ASHRAE. ASHRAE handbook- Heating, Ventilating, and Air-Conditioning Applications (SI Edition). Atlanta; 2021.

Bayer P, de Paly M, Beck M. Strategic optimization of borehole heat exchanger field for seasonal geothermal heating and cooling. Appl Energy. 2014;136:445–53.

Bayer P, Attard G, Blum P, Menberg K. The geothermal potential of cities. Renew Sustain Energy Rev. 2019;106:17–30.

Beck M, de Paly M, Hecht-Méndez J, Bayer P, Zell A. Evaluation of the performance of evolutionary algorithms for optimization of low-enthalpy geothermal heating plants. Proc 14th Int Conf Genet Evol Comput. 2012; p. 1047–54.

Cai W, Wang F, Liu J, Wang Z, Ma Z. Experimental and numerical investigation of heat transfer performance and sustainability of deep borehole heat exchangers coupled with ground source heat pump systems. Appl Therm Eng. 2019;149:975–86.

Cai W, Wang F, Chen S, Chen C, Liu J, Deng J, et al. Analysis of heat extraction performance and long-term sustainability for multiple deep borehole heat exchanger array: a project-based study. Appl Energy. 2021;289: 116590.

Chen C, Shao H, Naumov D, Kong Y, Tu K, Kolditz O. Numerical investigation on the performance, sustainability, and efficiency of the deep borehole heat exchanger system for building heating. Geotherm Energy. 2019;7(1):18.

Chen Y, Zhao Z, Peng H. Convective heat transfer of water flow in intersected rock fractures for enhanced geothermal extraction. J Rock Mech Geotech Eng. 2022;14(1):108–22.

Choi W, Ooka R, Nam Y. Impact of long-term operation of ground-source heat pump on subsurface thermal state in urban areas. Sustain Cities Soc. 2018;38:429–39.

Daemi N, Krol MM. Impact of building thermal load on the developed thermal plumes of a multi-borehole GSHP system in different Canadian climates. Renew Energy. 2019;134:550–7.

Gultekin A, Aydin M, Sisman A. Effects of arrangement geometry and number of boreholes on thermal interaction coefficient of multi-borehole heat exchangers. Appl Energy. 2019;237:163–70.

Kerme ED, Fung AS. Heat transfer simulation, analysis and performance study of single U-tube borehole heat exchanger. Renew Energy. 2020;145:1430–48.

Kindaichi S, Nishina D. Simple index for onsite operation management of ground source heat pump systems in cooling-dominant regions. Renew Energy. 2018;127:182–94.

Kolditz O, Bauer S, Bilke L, Böttcher N, Delfs JO, Fischer T, et al. OpenGeoSys: an open-source initiative for numerical simulation of thermo-hydro-mechanical/chemical (THM/C) processes in porous media. Environ Earth Sci. 2012;67(2):589–99.

Koohi-Fayegh S, Rosen MA. Examination of thermal interaction of multiple vertical ground heat exchangers. Appl Energy. 2012;97:962–9.

Lazzari S, Priarone A, Zanchini E. Long-term performance of BHE (borehole heat exchanger) fields with negligible groundwater movement. Energy. 2010;35(12):4966–74.

Liu X. An overview of EGS development and management suggestions. Front Res Archit Eng. 2020;3(3):6.

Liu L, Yu Z, Zhang H, Yang H. Performance improvements of a ground sink direct cooling system under intermittent operations. Energy Build. 2016;116:403–10.

Lucia U, Simonetti M, Chiesa G, Grisolia G. Ground-source pump system for heating and cooling: review and thermodynamic approach. Renew Sustain Energy Rev. 2017;70:867–74.

Lund JW, Toth AN. Direct utilization of geothermal energy 2020 worldwide review. Geothermics. 2021;90: 101915.

Luo J, Rohn J, Bayer M, Priess A, Wilkmann L, Xiang W. Heating and cooling performance analysis of a ground source heat pump system in Southern Germany. Geothermics. 2015;53:57–66.

Ma Y, Li S, Zhang L, Liu S, Liu Z, Li H, et al. Study on the effect of well layout schemes and fracture parameters on the heat extraction performance of enhanced geothermal system in fractured reservoir. Energy. 2020;202: 117811.

Ma J, Jiang Q, Zhang Q, Xie Y, Wang Y, Yi F. Effect of groundwater forced seepage on heat transfer characteristics of borehole heat exchangers. Geotherm Energy. 2021;9(1):11.

Menegazzo D, Lombardo G, Bobbo S, De Carli M, Fedele L. State of the art, perspective and obstacles of ground-source heat pump technology in the european building sector: a review. Energies. 2022;15(7):2685.

Meng B, Vienken T, Kolditz O, Shao H. Evaluating the thermal impacts and sustainability of intensive shallow geothermal utilization on a neighborhood scale: lessons learned from a case study. Energy Convers Manag. 2019;199: 111913.

Miglani S, Orehounig K, Carmeliet J. A methodology to calculate long-term shallow geothermal energy potential for an urban neighbourhood. Energy Build. 2018;159:462–73.

MOHURD. Ministry of Housing and Urban-Rural Development of China, Technical code for ground-source heat pump system (GB50366-2005), China Architecture Publishing and Media. China; 2009. https://www.antpedia.com/standard/5899942-1.html. Accessed 16 Mar 2023.

Noye S, Mulero Martinez R, Carnieletto L, De Carli M, Castelruiz AA. A review of advanced ground source heat pump control: artificial intelligence for autonomous and adaptive control. Renew Sustain Energy Rev. 2022;153: 111685.

Paly MD, Hecht-Méndez J, Beck M, Blum P, Zell A, Bayer P. Optimization of energy extraction for closed shallow geothermal systems using linear programming. Geothermic. 2012;43:57–65.

Sapińska-Sliwa A, Rosen MA, Gonet A, Kowalczyk J, Sliwa T. A new method based on thermal response tests for determining effective thermal conductivity and borehole resistivity for borehole heat exchangers. Energies. 2019;12(6):1072.

Schelenz S, Vienken T, Shao H, Firmbach L, Dietrich P. On the importance of a coordinated site characterization for the sustainable intensive thermal use of the shallow subsurface in urban areas: a case study. Environ Earth Sci. 2017;76(2):73.

Signorelli S, Kohl T, Rybach L. Sustainability of production from borehole heat exchanger fields. Twenty-Ninth Work. Geotherm Reserv Eng. Stanford, California; 2004. p. 26–8.

Song C, Li Y, Rajeh T, Ma L, Zhao J, Li W. Application and development of ground source heat pump technology in China. Prot Control Mod Power Syst. 2021;6(1):17.

Sun K. Analysis and evaluation of hydrogeological conditions of Beijing new airport terminal area. China Min Mag. 2021;30:275–95.
Tang B-J, Guo Y-Y, Yu B, Harvey LDD. Pathways for decarbonizing China's building sector under global warming thresholds. Appl Energy. 2021;298: 117213.
van der Zwaan B, Dalla LF. Integrated assessment projections for global geothermal energy use. Geothermics. 2019;82:203–11.
VDI. The Association of German Engineers (Verein Deutscher Ingenieure).Thermal use of the underground—Ground source heat pump systems. Beuth Verlag GmbH, Berlin.; 2019.
Wang Y, Wang Y, You S, Zheng X, Wei S. Operation optimization of the coaxial deep borehole heat exchanger coupled with ground source heat pump for building heating. Appl Therm Eng. 2022;213: 118656.
Yang W, Chen Y, Shi M, Spitler JD. Numerical investigation on the underground thermal imbalance of ground-coupled heat pump operated in cooling-dominated district. Appl Therm Eng. 2013;58(1–2):626–37.
Yang J, Xu L, Hu P, Zhu N, Chen X. Study on intermittent operation strategies of a hybrid ground-source heat pump system with double-cooling towers for hotel buildings. Energy Build. 2014;76:506–12.
You T, Wu W, Shi W, Wang B, Li X. An overview of the problems and solutions of soil thermal imbalance of ground-coupled heat pumps in cold regions. Appl Energy. 2016;177:515–36.
Yu M, Zhang K, Cao X, Hu A, Cui P, Fang Z. Zoning operation of multiple borehole ground heat exchangers to alleviate the ground thermal accumulation caused by unbalanced seasonal loads. Energy Build. 2016;110:345–52.
Zhang H, Han Z, Li X, Ji M, Zhang X, Li G, et al. Study on the influence of borehole spacing considering groundwater flow and freezing factors on the annual performance of the ground source heat pump. Appl Therm Eng. 2021;182: 116042.
Zhao T, Yu M, Rang H, Zhang K, Fang Z. The influence of ground heat exchangers operation modes on the ground thermal accumulation. Procedia Eng. 2017;205:3909–15.

Publisher's Note